Supercell-External Storms and Boundaries acting as Catalysts for Tornadogenesis

Jannick Fischer [a] and Johannes M. L. Dahl

Department of Geosciences, Texas Tech University, Lubbock, Texas

Corresponding author: Jannick Fischer, jannick.fischer@kit.edu

[a] Current affiliation: Institute of Meteorology and Climate Research - Department Troposphere Research (IMK-TRO), Karlsruhe Institute of Technology (KIT), Germany.

Early Online Release: This preliminary version has been accepted for publication in *Monthly Weather Review* cited, and has been assigned DOI 10.1175/MWR-D-22-0026.1. The final typeset copyedited article will replace the EOR at the above DOI when it is published.

ABSTRACT: It has long been observed that interactions of a supercell with other storms or storm-scale boundaries sometimes seem to directly instigate tornadogenesis. First, the authors explore the frequency of such constructive interactions. WSR-88D radar data are used to categorize 136 tornadic supercells into isolated supercells and supercells that interacted with external factors within 20 min before tornadogenesis. Most cases (80%) showed some form of external influence prior to tornadogenesis. Common patterns of interactions, the typical supercell quadrant that is affected, and changes in azimuthal shear are also identified. To further study these interactions, two sets of idealized CM1 simulations are performed. The first set demonstrates that the speed of the near-ground horizontal flow relative to the updraft can control whether a vortex patch develops into a tornado. A weaker updraft-relative flow is favorable because the developing vortex stays in the updraft region longer and becomes less tilted. Building on these results, it is shown that external outflow can lead to tornado formation by a deceleration of the updraft-relative flow. The deceleration is caused by the pressure gradient force associated with the external outflow, which is already noticeable several kilometers ahead of the outflow boundary. This offers another possible mechanism by which external outflow can act as a catalyst for supercell tornadogenesis.

Accepted for publication in *Monthly Weather Review*. DOI 10.1175/MWR-D-22-0026.1.

1. Introduction

The currently most prevalent conceptual model of supercell tornadogenesis is based on the evolution of a single, discrete supercell (e.g., Lemon 1976; Davies-Jones 2015). However, it is generally acknowledged among researchers and forecasters that storm-external factors can also have an impact on tornado formation. As discussed in this section, these external factors typically come in two forms; (i) supercell interaction with another thunderstorm, broadly referred to as storm merger events or (ii) supercell interaction with a pre-existing external boundary.[1]

a. Storm mergers

Early studies on severe thunderstorms investigated changes in storm characteristics after merger events [see the review articles by Hamilton (1969) and Westcott (1984)] and found significant impacts of mergers on supercell intensity, supercell structure and tornado potential. The most prominent example in the literature for the impact of storm mergers in tornadogenesis is perhaps the study by Lee et al. (2006), who focused on the 19 April 1996 Illinois tornado outbreak and showed that approximately 54% of tornadoes happened within 15 min of a cell merger. A similar percentage has been reported over multiple independent cases by Rogers and Weiss (2008), although the percentage was lower for significant tornadoes (27% for tornadoes rated EF2 or higher; Rogers 2012). This discrepancy seems consistent with the recent study by Flournoy et al. (2022), who analyzed a dataset of merger events, about half of which were associated with tornado reports (M. Flournoy, 2022, personal communication). For weak supercells, the merger tended to result in a strengthening of the low-level mesocyclone while stronger supercells more commonly experienced a weakening after the merger. They also found that an increase in azimuthal shear was more likely if multiple mergers were involved and over a longer duration.

Furthermore, a number of case studies have been published in which tornadogenesis seemed to be associated with the interaction and merging of a supercell with another thunderstorm (Dowell and Bluestein 2002a; Wurman et al. 2007; French et al. 2013; Weiss et al. 2015) or a squall line (Goodman and Knupp 1993). In an analysis of 21 squall line-supercell merger events, French and Parker (2012) found a maximum of tornado occurrences in the hour before the merger was complete,

[1]Changes in the environment over time (e.g., Coffer and Parker 2015; Klees et al. 2016) and supercell interaction with convective boundary layer features (e.g., Nowotarski et al. 2014) have also been shown to influence supercell structure. However, since these could be seen as properties of the respective environments, they are not specifically discussed here.

Accepted for publication in *Monthly Weather Review*. DOI 10.1175/MWR-D-22-0026.1.

leading them to speculate that "in cases where conditions may be favorable for tornado formation, the merger may in some way serve as an instigator." The term "catalyst" is preferred herein instead of "instigator" or "trigger", because it emphasizes that the merger is an *external* influence and more of a help than a necessary criterion for supercell tornadogenesis.[2] Throughout the literature, the term "merger" is only loosely defined and can either refer to the collision of the buoyant updrafts or the merging of the precipitation and outflow regions (e.g., Westcott 1984). Consequently, the hypothesized physical mechanisms by which storm mergers can influence tornadogenesis are also rather diverse, as described below.

For one, the coalescence of the buoyant thermals typically results in a single, more buoyant updraft (e.g., Wilkins et al. 1976; Lemon 1976). Furthermore, collision of the outflow of storm-mergers frequently causes new updraft development in a "bridge" between the two cells (e.g., Tao and Simpson 1984). Since the outflow characteristics (such as the amount of precipitation and evaporative cooling) often drastically change during a storm merger, Hastings and Richardson (2016) showed that the resulting increase in baroclinity can favor a stronger mesocyclone, which facilitates a stronger low-level updraft through the upward-directed nonlinear-dynamic pressure gradient force. Overall, these storm intensifications increase tornado potential due to the important role of the low-level updraft in intensifying near-ground rotation via vertical vorticity stretching (Markowski and Richardson 2014). Another type of factor is the direct influence of gust fronts associated with the outflow of merging storms. In the cases investigated by Wurman et al. (2007), a supercell repeatedly produced short-lived tornadoes at approximately the same times as the supercell merged with weaker storm cells moving in from the south. They hypothesized that the increase in convergence along the southern storms' outflows could have contributed to tornadogenesis. Recent numerical simulations by Honda and Kawano (2016) support this idea. A difficulty with predicting the outcome of a merger is that it can also weaken the resulting storm or disrupt ongoing tornadogenesis (e.g., Thompson and Edwards 2000; Bluestein and Weisman 2000; Wurman et al. 2007; French and Parker 2012; Klees et al. 2016), which is perhaps more common than a constructive merger (Flournoy et al. 2022). Furthermore, in hindsight it is often difficult to determine whether the storm merger actually played a role in tornadogenesis, or was just incidental (e.g., Tanamachi et al. 2015). The potential outcome of storm mergers depends on

[2]The analogy to a chemical catalyst is imperfect because the merging storm is usually not unchanged after the interaction.

Accepted for publication in *Monthly Weather Review*. DOI 10.1175/MWR-D-22-0026.1.

many factors, such as the distance, direction, and relative strength of the two cells [see Lee et al. (2006) and Hastings and Richardson (2016) for a detailed categorization of mergers].

b. Boundary interactions

A second common type of interaction of a supercell is with a local airmass boundary, which can be part of a synoptic front or produced by thunderstorm outflow. The observation that supercells frequently intensify and produce tornadoes when being close to a larger-scale boundary was already made based on early-generation radar and satellite data (e.g., Hamilton 1969; Purdom 1976). Maddox et al. (1980) analyzed multiple tornado outbreaks in the vicinity of boundaries and attributed the enhanced tornado risk to an increase in near-ground moisture, convergence, and vertical vorticity along the boundary. They furthermore concluded that stronger tornadoes were more likely in situations when the supercell travelled along the boundary instead of crossing it. Later studies suggested that the increased horizontal vorticity in vicinity of boundaries is a key factor through intensification of the mesocyclone (Markowski et al. 1998; Atkins et al. 1999; Rasmussen et al. 2000). In the VORTEX-95 cases analyzed by Markowski et al. (1998), around 70% of tornadoes happened near a boundary. In their statistic, they did not differentiate between synoptic-scale fronts and outflow boundaries, which also could have been associated with merger events. Similar to storm mergers, the interaction of a supercell with a boundary can also lead to a decrease in tornado potential (e.g., Blanchard 2008), especially if the storm quickly moves into colder surface air (Maddox et al. 1980; Doswell et al. 2002).

c. Research focus

The studies discussed thus far reveal storm mergers or boundary interactions can promote tornadogenesis and mostly attribute this to an intensification of the low-level updraft [step 3 of tornadogenesis in Davies-Jones (2015)]. Advances in our understanding of tornadoes suggest that a closer look at the vortex-scale dynamics might offer further insights. In observations, the position and movement of near-surface vertical vorticity maxima relative to the storm-scale updraft have been shown to have a large impact on tornado formation and maintenance (Dowell and Bluestein 2002b; Tanamachi et al. 2012; Skinner et al. 2014). In simulations, tornado-like vortices (TLVs) are often preceded by vortex patches or sheets in the supercell outflow (Markowski et al. 2014), which

Accepted for publication in *Monthly Weather Review*. DOI 10.1175/MWR-D-22-0026.1.

roll-up to symmetric vortices due to self-axisymmetrization (Dahl 2020) and undergo a transition of vorticity dynamics (Fischer and Dahl 2022). Several studies have shown that if the supercell low-level updraft is weak or not co-located with the near-ground circulation (e.g., Skinner et al. 2014; Markowski and Richardson 2014, 2017; Coffer and Parker 2017; Guarriello et al. 2018), or if the vortex patch moves out of the updraft area too quickly (e.g., Markowski and Richardson 2014; Fischer and Dahl 2020), the developing vortex dissipates. In a broad sense, this dissipation happens due to the increasing downward pressure gradient acceleration into the vortex core, which counteracts the upward-directed pressure gradient associated with the mesocyclone and ultimately causes a downdraft within the vortex (e.g., Markowski and Hannon 2006). In this way, which is sometimes described as “choking" or “vortex-valve effect" (Lewellen 1971; Lemon et al. 1975; Davies-Jones 1986, p. 224), vortex genesis often leads to its own demise. It seems that strong vertical pressure gradient accelerations due to the mesocyclone aloft are needed to overcome this effect and to sustain tornadogenesis (e.g., Coffer and Parker 2018). These ideas are consistent with observations of dissipating tornadoes, which are often displaced from the main updraft and vertically tilted (e.g., Golden and Purcell 1977; Bluestein et al. 2019; French and Kingfield 2019; Griffin et al. 2019). Therefore, a critical factor during tornadogenesis seems to be whether the developing vortex can stay in the main updraft region during the intensification period.

The purpose of this study is to apply these vortex-scale concepts in an effort to better understand supercell interactions with external factors. Specifically, this study investigates the question whether external outflow can aid in keeping the near-surface vortex patches within the updraft in situations where they would otherwise have moved away from it. In section 2, the study will be further motivated by quantifying how frequently such interactions could be responsible for tornadogenesis in a relatively large dataset of tornado cases and WSR-88D radar data. Then, sections 3a and 3b will present two sets of idealized simulations to further investigate the possible role of external outflow in supercell tornadogenesis. Sections 4 and 5 offer a discussion and summary of the results, respectively.

2. Observations

This analysis merely serves as an additional evidence for the frequency of external interactions in tornadic supercells, justifying looking at some details in simulations in section 3. Previous

Accepted for publication in *Monthly Weather Review*. DOI 10.1175/MWR-D-22-0026.1.

studies that offered a statistical analysis of external factors on tornadogenesis either looked at storm mergers (Lee et al. 2006; Rogers and Weiss 2008; Flournoy et al. 2022) or supercell interactions with boundaries (Markowski et al. 1998; Magee and Davenport 2020). However, storm mergers may also imply outflow interactions, even if these local cold pools are often chaotic and not clearly distinguishable on radar. Furthermore, one instigating mechanism for tornadogenesis, which will be proposed in section 3, seems possible with both larger-scale outflow-boundaries and local outflow from storm mergers. For these reasons, the goal of this section is to quantify how many tornadoes occur during or after any interaction with external storms *or* outflow boundaries. Synoptic boundaries are not included because their role in creating a locally more favorable environment for tornadogenesis (e.g., Maddox et al. 1980; Rasmussen et al. 2000; Magee and Davenport 2020) is not a focus of the simulation part of this study. The presented observations offer an analysis complementary to Flournoy et al. (2022), who filtered their dataset for merger events and then produced relevant statistics. The basis for our analysis is tornado reports and concurrent interactions such as mergers are analyzed.

a. Methods

The Storm Prediction Center tornado reports from 2015 to 2017 and during the Great Plains severe storms season (March–June) were used, accessed using the svrdb Python package (github.com/tsupinie/svrdb). Weather Surveillance Radar-1988 Doppler (WSR-88D) data were then manually analyzed for all tornado cases that fulfilled the following filtering criteria. (i) Only cases in the central Great Plains (between 32–43° north and 90–103° west) were used to focus on supercell tornadoes and reduce the number of mesoscale convective systems (MCSs), waterspouts, as well as coastal or orographic effects. The remaining non-supercell tornadoes were later manually removed from the dataset using radar reflectivity and velocity data. (ii) The reported starting location of the tornado was required to be less than 100 km from the nearest radar to have sufficient resolution and quality in the radar data. (iii) Only the first tornado of a supercell was analyzed to avoid the possibility that a previous tornado might have impacted the supercell structure and flow field. This was done by excluding all tornadoes that were preceded by another reported tornado within 90 min and 100 km. This filter was quite strict and likely removed many cases that could have been used, especially during tornado outbreaks. However, there is no obvious reason to

Accepted for publication in *Monthly Weather Review*. DOI 10.1175/MWR-D-22-0026.1.

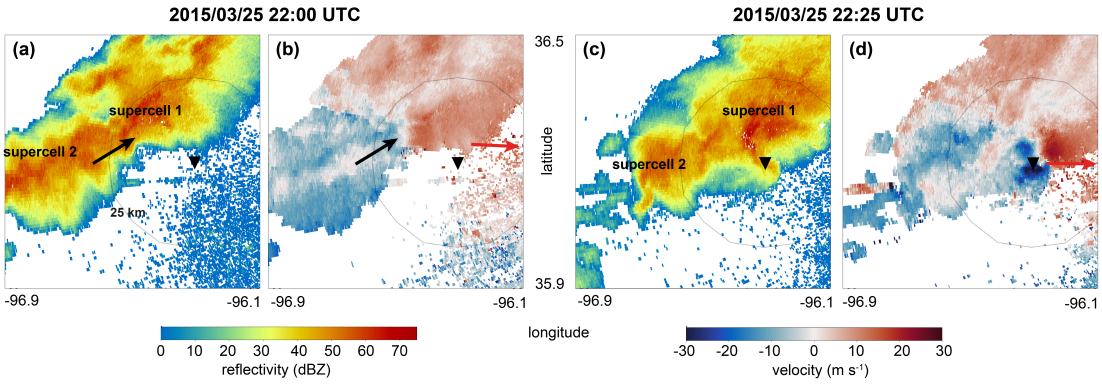

FIG. 1. Example analysis of 2015-03-25 at (a),(b) 22:00 UTC and (c),(d) 22:25 UTC, the scan immediately after tornadogenesis. The outflow from supercell 2 (indicated in the velocity field) impacted supercell 1 from the southwest. Subsequently, the mesocyclone in cell 1 intensified and a tornado was reported at 22:21 UTC. The black triangles show the location of the reported tornado and the thin black circle indicates a distance of 25 km from this location. The black arrow points to the tornadic supercell from the direction from which the external outflow influenced the supercell, thereby indicating the approximate angle of interaction (see text), which was estimated as 240°. The angle is more readily obtained when comparing all available radar scans (available at github.com/Janfisch/FischerDahl2022). The red arrow points in the direction of the radar.

assume that the interactions would have a different impact in these different scenarios. Therefore, and since abundant tornado cases were available, these strict criteria were preferred to make sure the analysis contained only the initial tornado that a supercell produced.

The 0.5° elevation angle radar reflectivity and radial velocity data were then analyzed using the Py-ART package (Helmus and Collis 2016). Cases for which radar data were not available or were erroneous, were excluded. All available radar scans (usually around 7–12 depending on the scanning interval, which varied between 3 and 7 min) within 35 min before and 10 min after the reported tornado were considered.

After all of the above filtering, 136 supercell tornado cases remained (20 cases were rated EF2 or higher). The cases were then manually categorized into (i) isolated supercells, and (ii) supercells that interacted with other storms or external boundaries before tornadogenesis. Cases were sorted into the latter category if a region with greater than 30 dBZ (indicating an external storm with significant intensity and outflow) or a fine line in radar reflectivity (indicating a mesocscale boundary) moved within 5 km of the relevant region of the supercell during the 20 min before the

Accepted for publication in *Monthly Weather Review*. DOI 10.1175/MWR-D-22-0026.1.

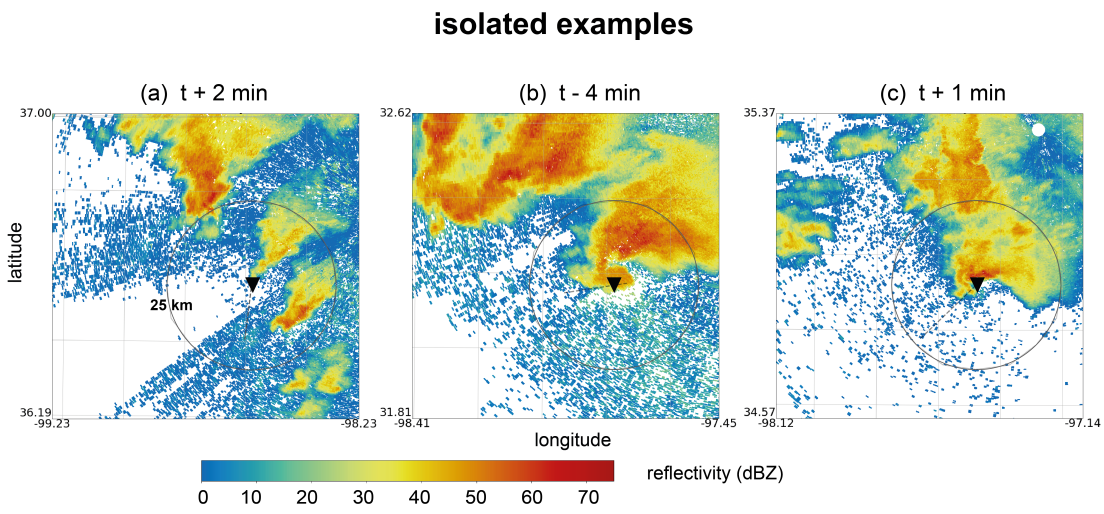

FIG. 2. Examples for cases that were categorized as isolated supercells. The scans shown were chosen to best represent the respective case and are at (a) 2015-04-18 21:08 UTC, (b) 2015-04-27 at 02:05 UTC, (c) 2015-05-19 19:41 UTC. The time relative to the tornado report (t) is indicated near the top of each panel. The calculated path of the supercell (see text) is shown as a thin dashed line. All other markers are as in Fig. 1.

tornado report.[3] Hence, features included whole-storm mergers, but also radar-detected boundaries and flanking-line cells or other prolonged convection that affected the tornadic supercell. This approach ensured that all possible interactions with radar-detectable storms and outflow were included. Figure 1 provides a detailed example for the analysis, and Figs. 2 and 3 show reflectivity snapshots of example cases of both isolated and non-isolated storms. Animations for all the example cases can be viewed online at github.com/Janfisch/FischerDahl2022.

Additionally, the angle at which a boundary or a merging storm impacted the tornadic supercell was estimated manually by drawing a line from the interacting feature to the supercell mesocyclone using the radar scans prior to the interaction. The storm motion of the supercell was taken into account to make the angle storm relative. For instance, the outflow of supercell 2 in Fig. 1 impacted supercell 1 from the southwest because both supercells moved in parallel to each other and the outflow spread out from supercell 2. The goal of this analysis was not to obtain exact angles, which would have been impossible given the complexity and data limits, but to broadly estimate a direction from which most interactions originated.

[3]This range in space and time was chosen to be consistent with the simulations in section 3. The "relevant" region where the tornado formed was typically the hook echo (in reflectivity) and mesocyclone region (couplet in radial velocity).

Accepted for publication in *Monthly Weather Review*. DOI 10.1175/MWR-D-22-0026.1.

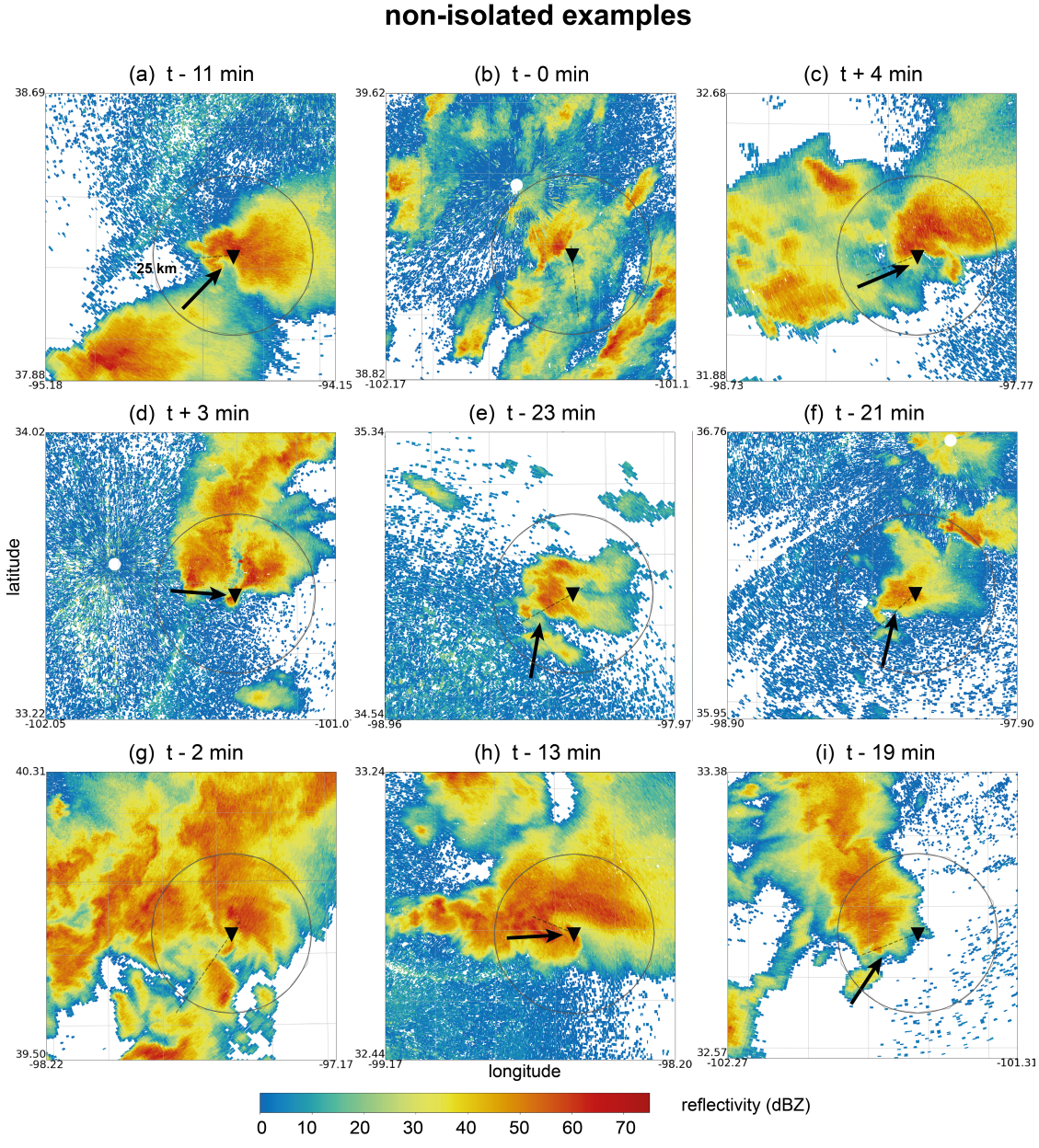

FIG. 3. As Fig. 2 but for cases that were categorized as non-isolated. The scans shown were chosen to best represent the case and are at (a) 2015-04-08 2:42 UTC, (b) 2015-04-17 23:55 UTC, (c) 2015-04-27 0:02 UTC, (d) 2015-05-06 0:27 UTC, (e) 2015-05-06 19:21 UTC, (f) 2015-05-06 21:16 UTC, (g) 2015-05-07 0:12 UTC, (h) 2015-05-26 02:26 UTC, (i) 2015-05-28 20:08 UTC. The arrows indicate the approximate direction from which the external storm or boundary influenced the supercell. (b) and (g) represents case in which no angle could be determined because the interactions were too complex.

Accepted for publication in *Monthly Weather Review*. DOI 10.1175/MWR-D-22-0026.1.

Lastly, to compare this dataset to the cases in Flournoy et al. (2022), changes in azimuthal shear over time (in their analysis used as a proxy for supercell intensity) were determined for all cases. Azimuthal shear was calculated from the 0.5° elevation angle radial velocity data in Py-ART. A distance-weighted average interpolation (Barnes 1964) to a cartesian grid with 0.005° grid spacing was used to smooth the data prior to the analysis. This provided similar azimuthal shear fields as in the MYRORSS dataset used in Flournoy et al. (2022), which was unfortunately not available between 2015-2017. The azimuthal shear value range was slightly larger in the present dataset, presumably because of differences in the smoothing. Like in Flournoy et al. (2022), the azimuthal shear analysis was carried out by manually tracking the supercells backwards (using radar reflectivity and velocity images to follow the hook echo and mesocyclone region) to the radar scan closest to 30 min before the tornado report. Then, a linear storm motion vector was calculated between this location to the reported tornado. Adding this storm motion in each radar scan resulted in an approximated supercell path (Figs. 2 and 3). The maximum azimuthal shear within a radius of 5 km from this location was then determined for each radar scan, resulting in a time series of maximum azimuthal shear for each supercell.

b. Results

The analysis revealed that 109 of 136 supercell tornadoes (80%) were categorized as "non-isolated" and 27 (20%) as "isolated". For the tornadoes rated EF2 or higher, the percentage of non-isolated supercells was likewise 80% (16 of 20). Two other scientists that were enlisted by first author confirmed this assessment.[4] Since some of the interactions were likely coincidental, this percentage should be seen as an upper bound for the potential influence of these external factors. Further discussion and comparison with previous literature can be found in section 4.

Several patterns of interaction that were commonly observed are briefly described below: (i) A chain of two or more supercells, with the southern cell "pumping" outflow into the northern tornadic cell (Fig. 1a-d and Fig. 3a,c). (ii) A QLCS or outflow boundary impacting a supercell from the West (Fig. 3d). (iii) A previously discrete storm merging with the supercell either before or during tornadogenesis. In many cases these were relatively small cells merging in the supercell inflow region (Fig. 3e,f). (iv) Convection along the flanking line of the supercell, with the flanking-line storms producing outflow that influenced the supercell (Fig. 3h,i).

[4]The percentages of non-isolated supercells were 86 and 82% in these independent assessments.

Accepted for publication in *Monthly Weather Review*. DOI 10.1175/MWR-D-22-0026.1.

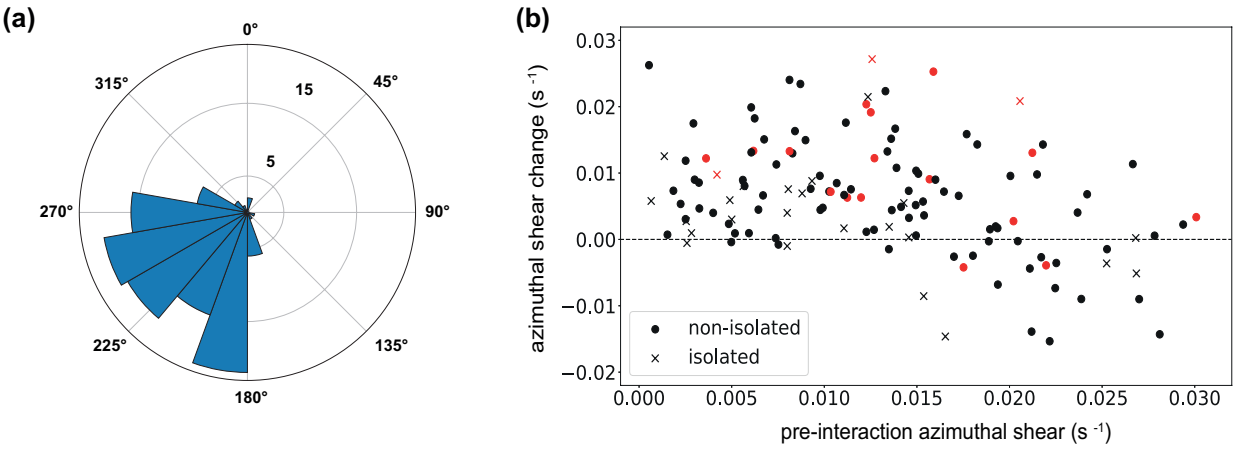

FIG. 4. (a) For the 109 supercells with external influence, the angle from which the external boundary or cell moved into the region of tornadogenesis is shown, binned in 20° increments (from initial 5° estimates). The angles start at 0° north and are storm relative, so e.g., an influence directly from the south would correspond to a angle of 180°. (b) Scatterplot of all 136 cases, showing the difference in azimuthal shear between the radar scan immediately before the tornado report (using the radar scan after the tornado report instead did not meaningfully change the results) and the scan closest to 30 min before the report (y-axis) as a function of the latter value (x-axis). Circles show the non-isolated cases and crosses the isolated ones. Red coloring indicates cases with tornadoes rated EF2 or higher.

A distribution of the approximate angles at which external cells or boundaries impacted the supercells is shown in Fig. 4a. Almost all interaction prior to tornadoes happened from the southwestern quadrant. This result is consistent with Rogers and Weiss (2008) and the rear-flank mergers investigated by Hastings and Richardson (2016).

Figure 4b, which is comparable to Fig. 11 by Flournoy et al. (2022), shows that the vast majority of cases featured an increase in azimuthal shear over the 30 min before tornadogenesis. This is perhaps not surprising considering that all cases became tornadic. In other words, only constructive interactions were included here, in contrast to both constructive and destructive merger-events included in Flournoy et al. (2022). Similar to their results, a decrease in azimuthal shear (in their analysis interpreted as a destructive merger) was more frequent if the mesocyclone was already strong before the interaction. However, this trend is also found in the isolated cases here, which suggests that it might be more of a data artifact than a physical relationship. It is acknowledged, however, that the isolated supercell dataset is small and hence might not be as statistically robust and

Accepted for publication in *Monthly Weather Review*. DOI 10.1175/MWR-D-22-0026.1.

that the non-isolated category is not identical to the merger cases in Flournoy et al. (2022). Lastly, no obvious relationship between tornado intensity and azimuthal shear change was found (Fig. 4b). Overall, the observations emphasize that interactions are common prior to tornadogenesis. One way such interactions might facilitate tornadogenesis will now be studied with idealized simulations.

3. Idealized simulations

In this section, two different idealized simulation approaches are used to further investigate the possibility that supercell-external factors sometimes serve a catalysts for tornado formation. First, it is shown why tornadogenesis might fail in a highly idealized scenario. These results are then used to understand the impact of external outflow on tornadogenesis.

a. The impact of varying near-ground updraft-relative flow

1) Model setup

The goal of this section is to shed more light on the near-ground vortex dynamics during tornadogenesis in different updraft-relative flow situations. A highly idealized simulation approach was chosen, using CM1 (Bryan and Fritsch 2002) version 19.5. The horizontal grid spacing was 100 m in the central domain with a horizontal dimension of 15 km × 15 km and then stretched to 500 m near the outer domain boundary with a total size of 60 km × 60 km. The vertical grid spacing was 20 m in the lowest 600 m and then stretched to 180 m between 600 and 5600 m (model top). The Coriolis parameter was set to zero. Since the focus was on the tornadogenesis period and not a realistic representation of the developed TLV structure, the free-slip bottom boundary condition was used (see e.g., Fischer and Dahl 2022).[5] The model configuration and base-state potential temperature profile (constant $\partial\theta/\partial z$) were based on the idealized simulations in Fischer and Dahl (2022). The setup is shown in Fig. 5a. A constant heat source was used to generate a strong updraft in the lowest few kilometers [S_{w0} = 0.08 K s^{-1}; x_w = -1000 m, y_w = 0 m, z_w = 700 m, horizontal radius R_w = 2000 m, vertical radius Z_w = 500 m; see Markowski and Richardson (2014) and Fischer and Dahl (2020) for details]. The simulations were dry and no heat sink was employed, hence no cold outflow was present. After 620 s, when the updraft was fully developed, an elliptical vortex patch was artificially added in the lowest 400 m, identical to the one used in

[5]Using semi-slip the results did not meaningfully change.

Accepted for publication in *Monthly Weather Review*. DOI 10.1175/MWR-D-22-0026.1.

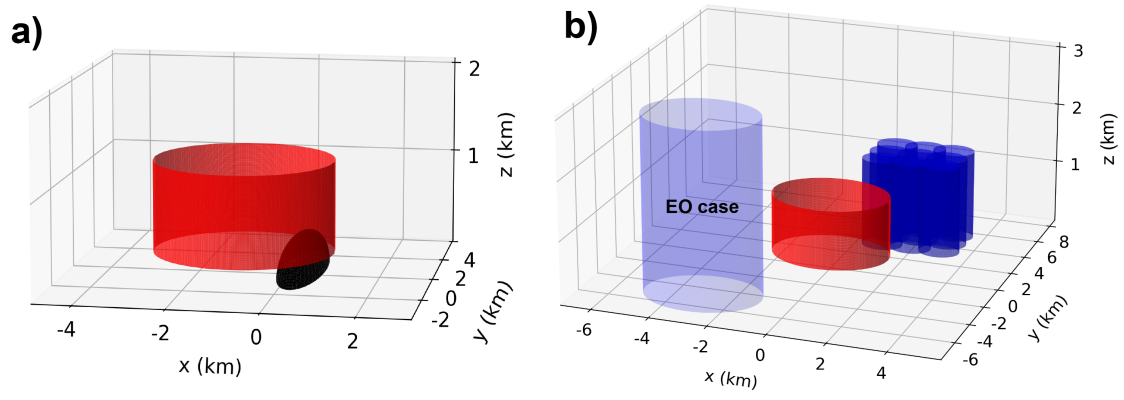

FIG. 5. Idealized model setups for (a) the evolution of an elliptical vortex patch below an updraft in section 3a and (b) simulations with external outflow as opposed to without one in section 3b. Heat sources are illustrated as red cylinders, heat sinks as blue cylinders and the artificial vortex patch as black ellipsoid.

Fischer and Dahl (2022) (x = 300 m, y = 100 m, D_{major} = 4 km, D_{minor} = 1 km; $\zeta_{max} = 0.03\ s^{-1}$). This vortex patch then rolled up to a rather symmetric vortex while intensifying. The simulations were run for 1800 s.

An additional layer of complexity was added to this idealized tornadogenesis model by conducting four CM1 runs with different near-ground wind speeds relative to the stationary heat source. In the control simulation (SR3), a uniform easterly wind of $u_0 = -3\ m\ s^{-1}$ was used as by Fischer and Dahl (2022). In the three additional runs, the magnitude of the easterly storm-relative wind was increased linearly toward the surface in the lowest 400 m, (see insets in Fig. 6), so that $u_0(z = 0)$ = -6 m s^{-1} (SR6), -9 m s^{-1} (SR9) and -12 m s^{-1} (SR12) at the surface, respectively.[6] Hence, the four simulations had varying degrees of near-ground updraft-relative easterly winds between 3 and 12 m s^{-1}, representing different flow situations of supercell outflow relative to the updraft. This led to different advection speeds for the vortex patch during its roll-up to a TLV.

2) RESULTS

In all four cases, after initialization of the vortex patch, the vertical-vorticity-rich air was quickly ingested into the updraft and the vortex patch rolled up and was advected vertically over a depth of several km, similar to Fischer and Dahl (2022). As discussed in their study, this implies vertical

[6]This was realized by having a domain motion of u = 3 m s^{-1} and adding a layer of linearly increasing winds with height in the lowest 400 m. The different wind profiles led to small changes in the shape of the updrafts (Fig. 6) but the influence on the updraft strength was small in the area of the vortex.

Accepted for publication in *Monthly Weather Review*. DOI 10.1175/MWR-D-22-0026.1.

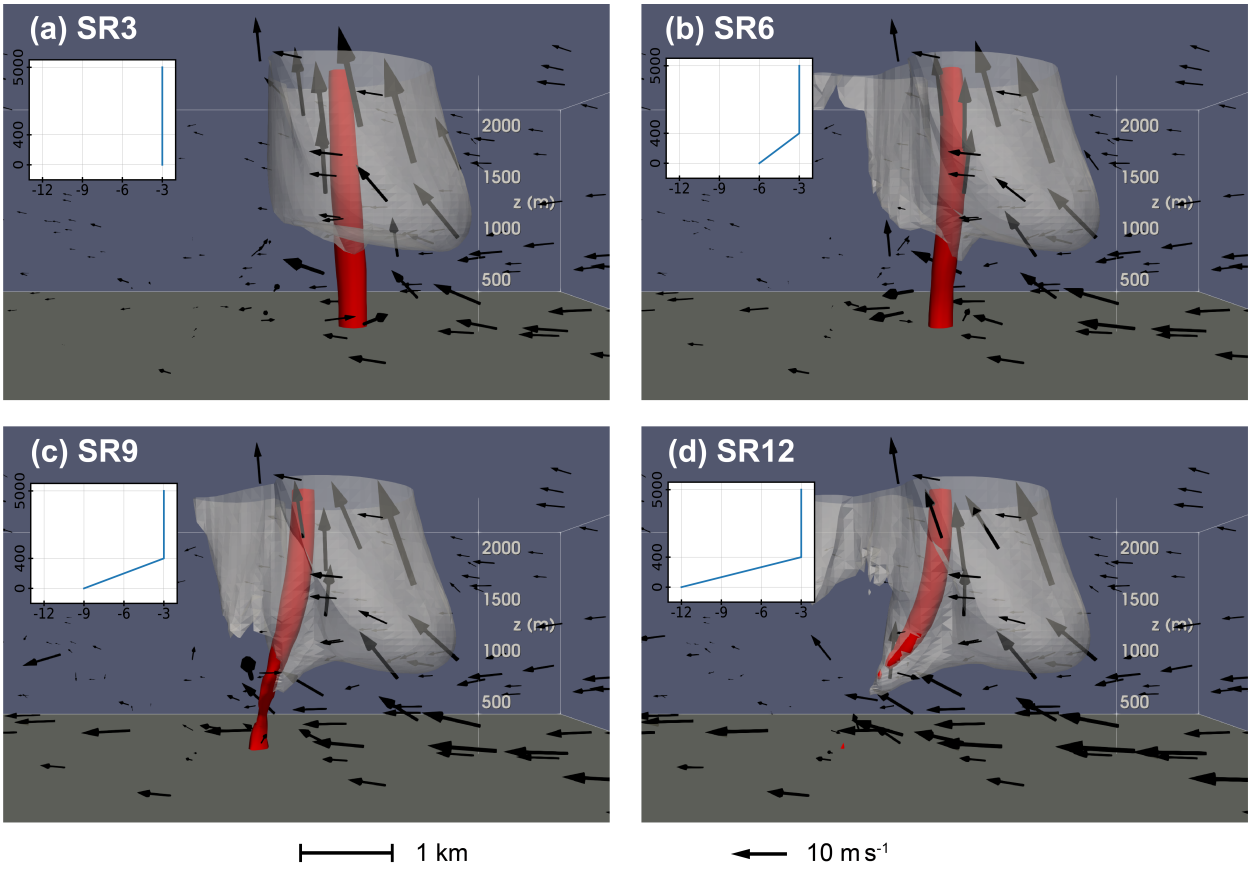

FIG. 6. (a) SR3, (b) SR6, (c) SR9 and (d) SR12 simulations at 900 s. Vertical velocity (10 m s^{-1} contour in grey), vertical vorticity (0.1 s^{-1} contour in red), velocity vectors (black). Only data below 2.5 km AGL is shown. The vector positions follow a uniform spatial distribution. The small insets in each corner show the wind profile of each simulation in m s^{-1}. Note that the y-axes (in m) in the insets are not uniformly scaled and that in the 3D visualizations the scale vector and distance markers may slightly vary in accuracy because of the visual distortion.

vorticity stretching and vortex symmetrization. Figure 6 shows the four cases at 900 s (an animation of the full evolution is available under github.com/Janfisch/FischerDahl2022). In the cases with larger updraft-relative flow speed, the near-ground vortex was advected away from the updraft relatively quickly, while the upper part of the vortex stayed rooted in the updraft. The TLVs in SR3 and SR6 were the strongest and most vertically coherent (Fig. 6a,b). In the SR9 run, the near-ground circulation was displaced around 600 m farther west than aloft. Therefore, the vortex was slightly tilted between around 0 and 1.5 km AGL (Fig. 6c). At these lower levels, the vortex was also much weaker and the largest vertical vorticity was found farther aloft. These differences

Accepted for publication in *Monthly Weather Review*. DOI 10.1175/MWR-D-22-0026.1.

were even more pronounced in the SR12 run, in which the vertical vorticity mostly stayed below 0.1 s^{-1} in the lowest km (Fig. 6d and Fig. 7a). Figure 7 shows that this weaker rotation is likely attributable to the transport of the low-level vortex out of the main area of convergence (the largest surface convergence is near the vortex itself and disturbances in the flow in the lee of the updraft while broad and deep convergence is only found near the heat source).

These characteristics seem consistent with some funnel clouds in observations of tornadogenesis failure (e.g., Tanamachi et al. 2013). Here the vortex visibly rotates near the cloud base and is often vertically tilted (Fig. 8). The simulations suggest that a closed circulation through all levels is likely present in these cases. However, the circulation can have vertically varying intensity. The rotation aloft (e.g., in area of the funnel) can be much stronger than near the ground (Fig. 7a, also see Fig. 6d and Fig. 8a). Alternatively, the vortex can be relatively strong aloft and at the ground, but weaker in between (Fig. 7b, also see Fig. 6c and Fig. 8b), likely because the convergence field close to the ground is at times locally (e.g., close to the vortices; see Fig. 7) decoupled from the convergence farther aloft associated with the main updraft. Consistent with observations (e.g., Tanamachi et al. 2013), this suggests that damaging winds are possible near the ground, even if no funnel is observed and no rotation is detected at the lowest radar scan.

Throughout the rest of the simulation, the TLV dissipated first in the SR12 run and then in the SR9 run, due to an increasing displacement of the near-ground vortex from the main updraft. In the SR6 run, the vortex persisted throughout the whole simulation but also slowly moved west at all levels, away from the stronger updraft, resulting in a gradual decrease in TLV intensity. These later stages of the simulations might be slightly influenced by the different shapes of the updraft with the different wind profiles (see e.g., Fig. 6) but these vertical velocitiy differences tended to be small and the vortices themselves also had some influence on the updraft structure.

Overall, these idealized simulations demonstrate the importance of the storm-relative advection of the developing vortex, which has previously been indicated in observations (e.g., Dowell and Bluestein 2002b; Tanamachi et al. 2012; Skinner et al. 2014) and simulations (e.g., Markowski and Richardson 2014; Guarriello et al. 2018; Murdzek et al. 2020; Gray and Frame 2021). The results are important in light of the main research focus of this study because any external factors that could influence the near-ground flow could thereby also influence tornadogenesis. In the following, this possibility will be explored with a second set of simulations.

Accepted for publication in *Monthly Weather Review*. DOI 10.1175/MWR-D-22-0026.1.

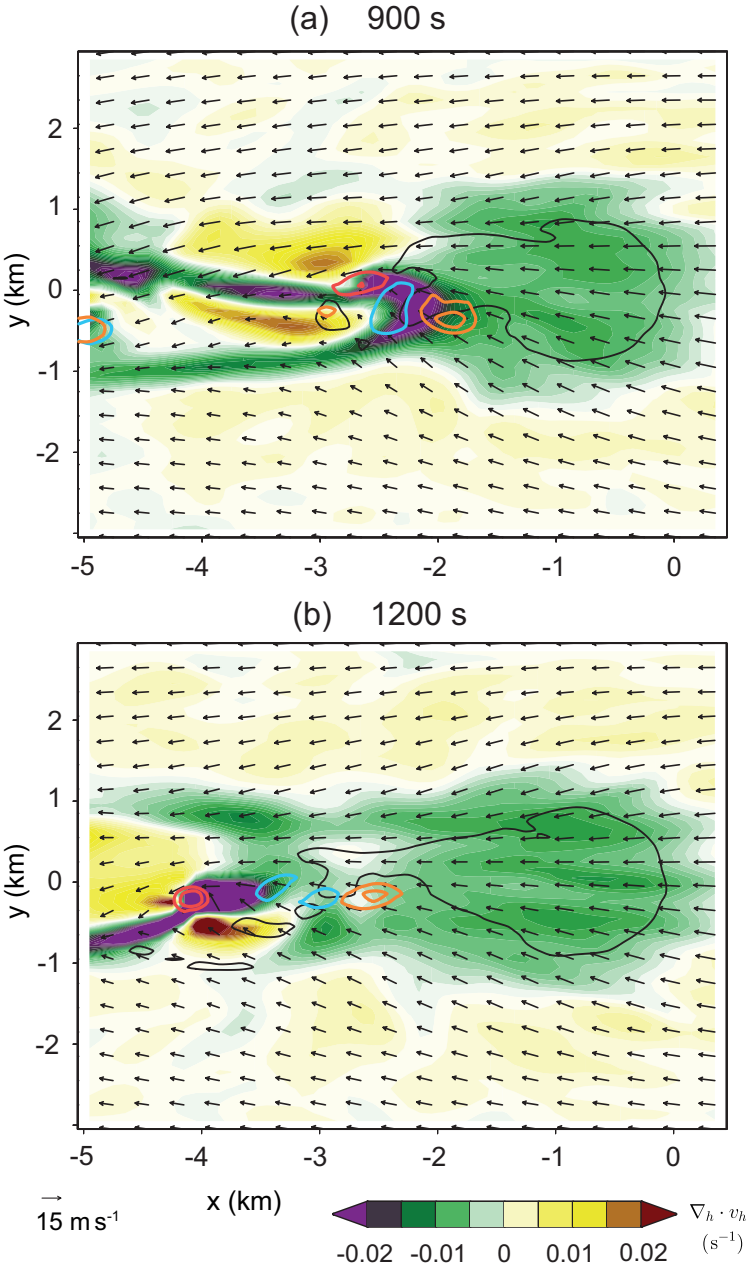

FIG. 7. SR12 simulation at (a) 900 s and (b) 1200 s. Horizontal divergence at 10 m AGL is shaded and at 590 m contoured black (-0.01 s^{-1}). Vertical vorticity is contoured at 0.05 and 0.1 s^{-1} at three different levels, 10 m (red), 590 m (teal), and 1200 m (orange). Horizontal wind vectors at 10 m AGL were also added.

b. External outflow acting as catalyst for tornadogenesis

The previous section supports the idea that the duration that intensifying vortices spend below a sufficiently strong updraft region is critical for tornadogenesis. The updraft-relative flow appears

Accepted for publication in *Monthly Weather Review*. DOI 10.1175/MWR-D-22-0026.1.

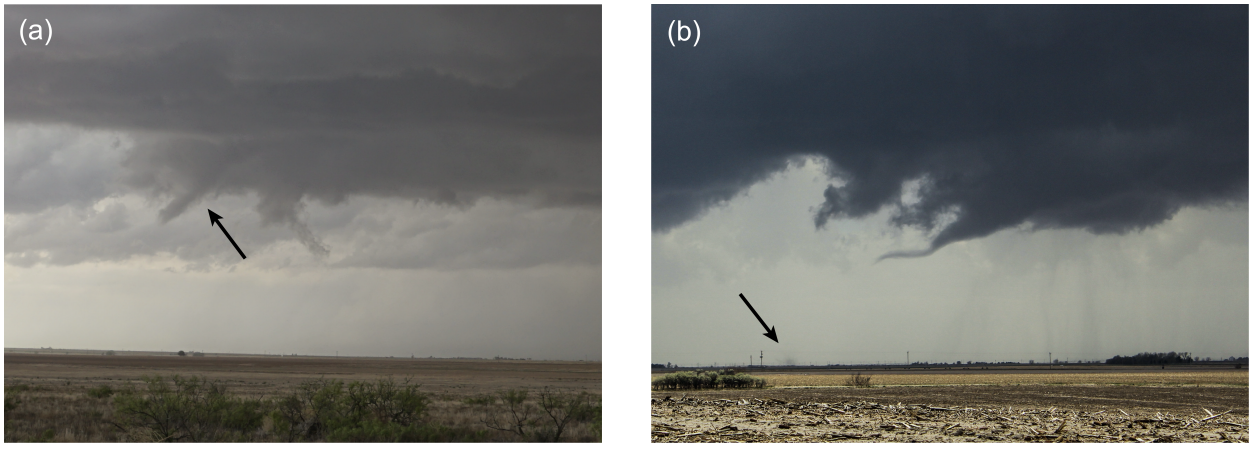

FIG. 8. (a) Short-lived funnel cloud (black arrow) with no noticeable ground circulation. Photo courtesy of Jannick Fischer. (b) Vertically tilted funnel cloud. Weak ground circulation can be observed towards the bottom left (black arrow). Photo courtesy of Alex Schueth.

to be an important factor in this regard. The equivalent in real supercells is the outflow air, in which the developing tornado would be embedded (e.g., Markowski and Richardson 2014). This section explores how this near-ground flow in the updraft region could be altered by *external* outflow, thereby influencing tornadogenesis.

1) MODEL SETUP

It is reasonable to assume that an instigating mechanism for tornadogenesis would only work if the parent supercell already had the general potential to produce a tornado (e.g., Goodman and Knupp 1993; French and Parker 2012). Therefore, using supercell simulations to analyze a potential instigating effect of storm mergers is difficult, because it is somewhat subjective whether the modeled supercell has tornado potential or not at a given time. For this reason, this section used the idealized setup of Fischer and Dahl (2020), in which the tornadic and nontornadic cases were clearly separated and depended on the prescribed updraft and cold pool strengths (their Fig. 15).

The CM1 configuration is similar to the one in section 3a, except that near-ground vertical vorticity was generated in outflow air by employing an array of heat sinks northeast of the heat source [Fig. 5b; see Fischer and Dahl (2020) for more details]. This setup resulted in a complex outflow structure and the repeated generation of vortex patches [following the downdraft mechanism based on reorientation of baroclinically generated horizontal vorticity in descending parcels (Davies-

Accepted for publication in *Monthly Weather Review*. DOI 10.1175/MWR-D-22-0026.1.

Jones and Brooks 1993; Dahl et al. 2014; Dahl 2015; Parker and Dahl 2015; Fischer and Dahl 2022)]. A simulation from Fischer and Dahl (2020) with a heat source strength of $S_{w0} = 0.08$ K s^{-1} and heat sink strength of $S_{c0} = -0.0105$ K s^{-1} was chosen as control run here, serving as a representative example of a barely nontornadic simulation.

In a restart run of this control simulation, a large and constant heat sink (x = -3 km, y = -5 km, z = 0 km; R_w = 2 km, Z_w = 3 km; $S_{c0} = -0.01$ K s^{-1}) was started at 1 h simulation time in the area southwest of the updraft (Fig. 5b). This heat sink generated a growing cold pool, thereby mimicking the impact of an external outflow boundary or the outflow of a storm merger on the supercell-like pseudostorm from the southwest. Therefore, this second simulation will be referred to as the external outflow (EO) run.

2) Results

The control simulation remained nontornadic over the whole 2 h simulation time (< 0.2 s^{-1}). As discussed by Fischer and Dahl (2020) and shown in Figs. 9a,c,e,g, TLV genesis failed because the vortex patches did not fully intensify to TLV strength before being advected out of the updraft area (note the similarity of tornadogenesis failure to e.g., the SR3 run in section 3a). However, the pseudostorm could be seen as being on the verge of becoming tornadic, because simulations with only slightly stronger heat source and heat sink strength produced a TLV [see Fig. 15 in Fischer and Dahl (2020)]. Therefore, this control run served as an ideal comparison to the EO run to test the possible impacts of external outflow.

In the EO run, the additional heat sink generated a strong cold pool (minimum potential temperature perturbation around -5 K) which spread northeast against the surrounding flow into the updraft area of the pseudo-supercell. In Figure 9b, the still weak external outflow can be seen in the southwestern corner 600 s after the restart. The vorticity and horizontal velocity fields in the updraft area were still quite similar between the two simulations at this time. Another 300 s later at 4500 s (Fig. 9d), more differences appeared in the EO run, with the wind field in the region southwest of the vortex patch attaining a more westerly component and the vortex patch staying a few hundred meters farther northeast, being less tilted with height, and slightly stronger. These differences became more pronounced over the next 300 s (Fig. 9f). Furthermore, the vortex patch developed into a symmetric TLV around this time, with a rapid pressure decrease in the core

Accepted for publication in *Monthly Weather Review*. DOI 10.1175/MWR-D-22-0026.1.

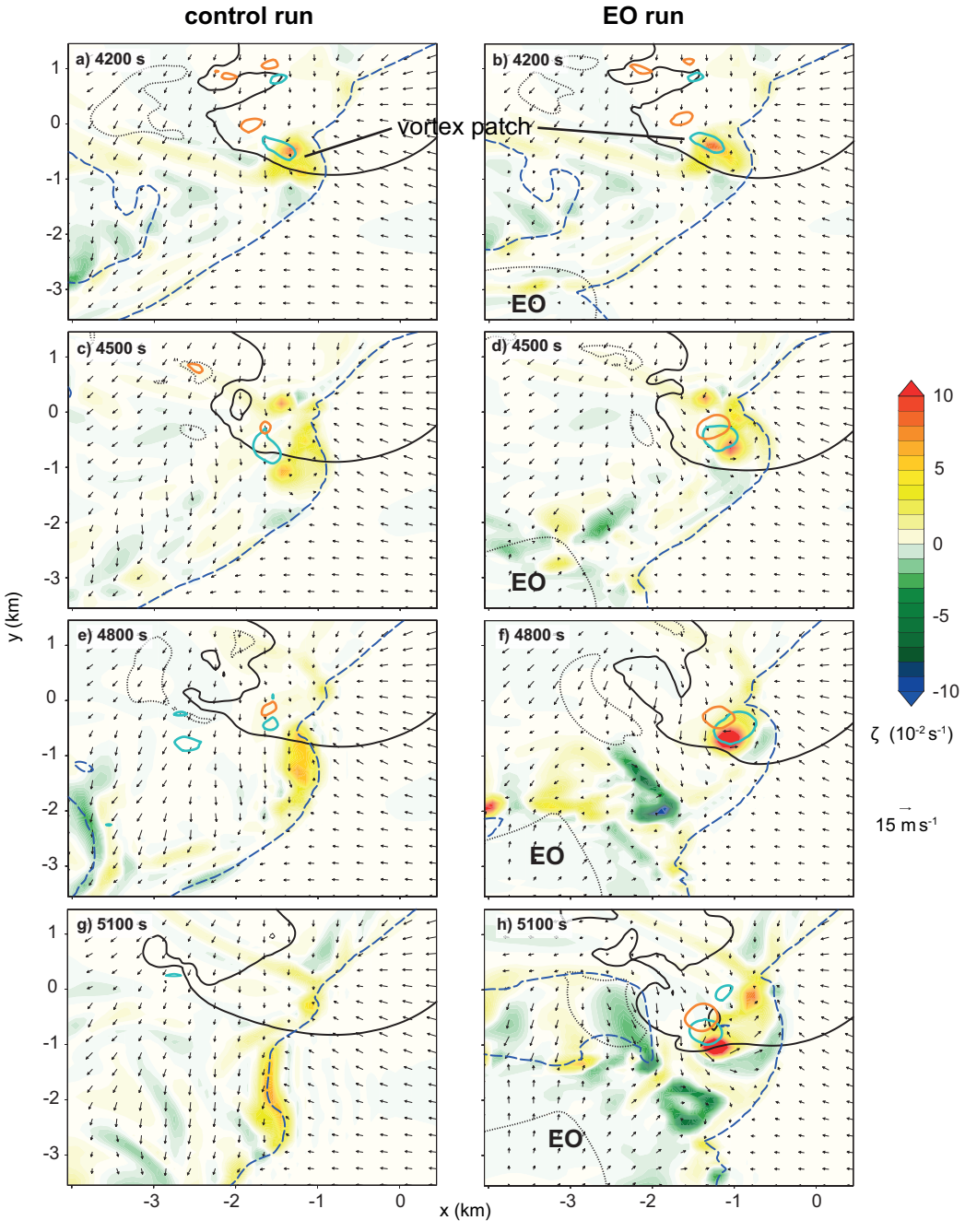

FIG. 9. Comparison of the control run (left column) and the external outflow run (right column) at (a),(b) 4200 s , (c),(d) 4500 s, (e),(f) 4800 s and (g),(h) 5100 s. Vertical vorticity is shaded at 30 m AGL and contoured at 590 m (teal) and 1.2 km (orange). The 30 m AGL -1 K potential temperature contour is indicated in blue and horizontal wind vectors are shown. Vertical velocity at 1.2 km is contoured in black (+3 m s^{-1} solid, -3 m s^{-1} dotted). The area with external outflow is labeled with "EO."

Accepted for publication in *Monthly Weather Review*. DOI 10.1175/MWR-D-22-0026.1.

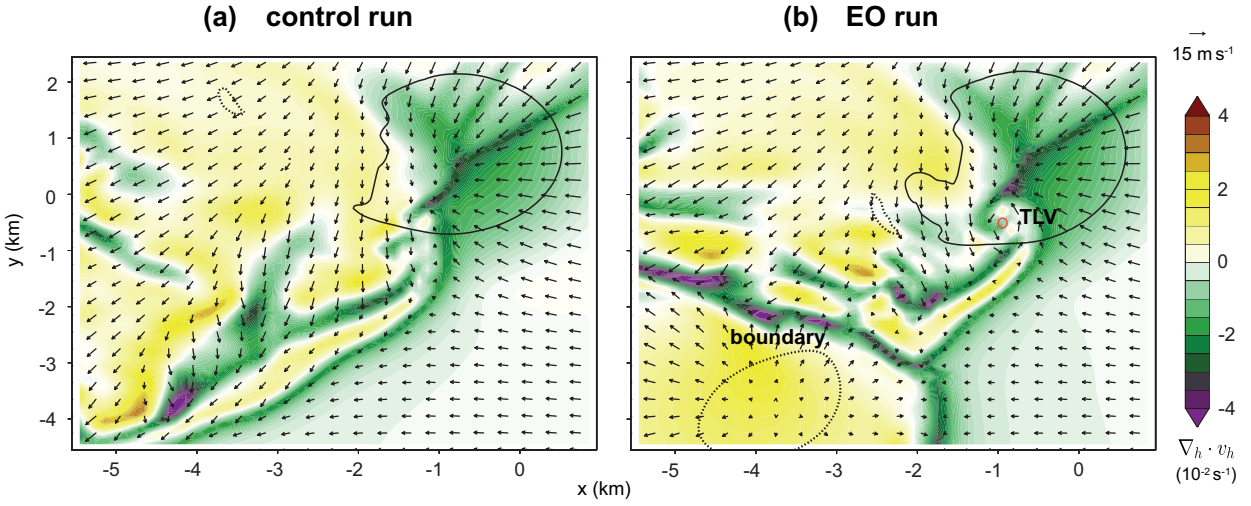

FIG. 10. Comparison of (a) the control run and the (b) external outflow run at 4680 s when the TLV was rapidly intensifying and just reached <1 hPa p' (red contour). Divergence at 30 m AGL is shaded. Vertical velocity at 1.2 km AGL is contoured in black (+3 m s^{-1} solid, -3 m s^{-1} dotted). The TLV and the boundary between the two outflow areas are labeled.

(Fig.10b). At 5100 s (Fig. 9h), the TLV weakened before it recycled into an even stronger TLV a few minutes later, which persisted throughout the rest of the EO run. In contrast, the vortex patch in the control run was already advected a few km farther downstream and rather asymmetric (Fig. 9g).

The change of tornado potential between the control and EO run can only be a result of the additional heat sink and resulting external outflow, because all other parameters were identical. This is perhaps surprising because the external outflow boundary stayed several kilometers southwest of the updraft throughout the period discussed. Therefore, enhanced convergence, as suggested by Wurman et al. (2007) and Honda and Kawano (2016), can not be the reason for why a TLV formed here. This is supported by Figure 10, which shows that the near-ground convergence is similar in the two simulations in the vicinity of the TLV and convergence along the external outflow boundary is only enhanced around 2 km southwest of the developing TLV. It appears instead that the added heat sink caused changes in the flow *ahead of the actual boundary*, which resulted in the vortex patch remaining in the updraft region for a longer time. To explain this rather passive influence, the perturbation pressure field is analyzed next.

Accepted for publication in *Monthly Weather Review*. DOI 10.1175/MWR-D-22-0026.1.

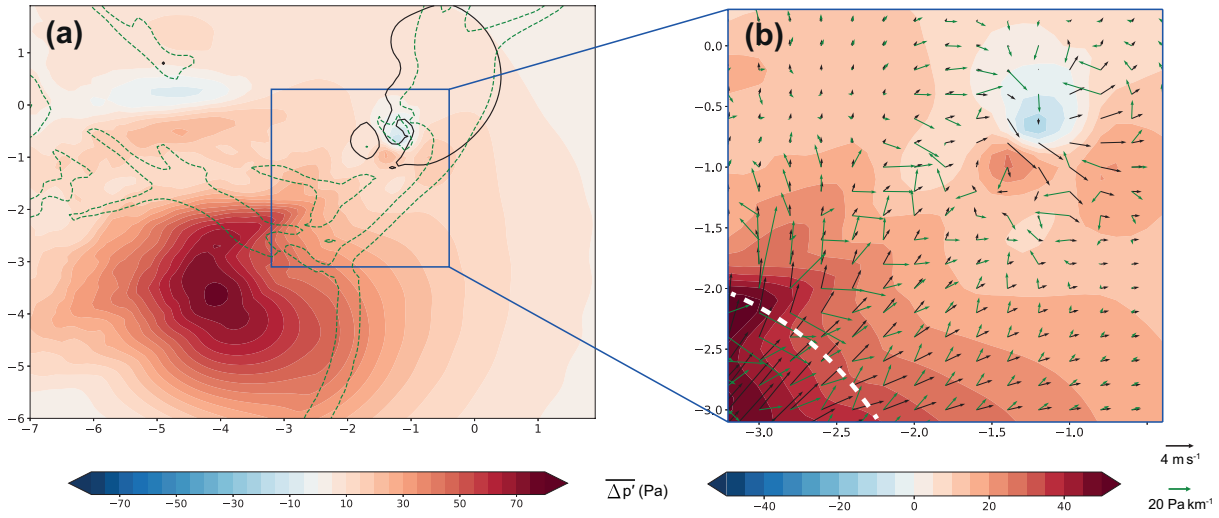

FIG. 11. Difference in the 30 m AGL perturbation pressure field between the external outflow run and the control run (shaded), averaged between 3900 and 4500 s (the period 10 min before tornadogenesis). In (a), the 30 m AGL horizontal convergence (0.01 s^{-1} dashed green) and the 500 m AGL vertical velocity (3 m s^{-1} black) at 4500 s in the EO run were added as visual reference. In (b), a smaller region around the vortex patch is shown. The green vectors at every second grid point represent the gradient of the shaded pressure difference field, i.e., the difference in the averaged pressure gradient between the simulations. The black vectors represent the vector difference of the horizontal wind between the two runs averaged over the same time. The white dashed line indicates the approximate location of the gust front at 4500 s.

Figure 11a shows that the external outflow was associated with an average high pressure perturbation near the ground, consistent with what would be expected from the hydrostatic pressure increase due to larger density in the cooled region. However, the positive pressure perturbation extended beyond the external outflow and hence several kilometers ahead of the gust front (Fig. 11b). This pattern is consistent with 2D simulations of density currents (e.g., Markowski and Richardson 2010, their Fig. 2.6) and likely dominated by the dynamic (non-hydrostatic) forcing by the interaction of the outflow boundary with the opposing flow (Droegemeier and Wilhelmson 1987). This conclusion is supported by Fig. 12 which shows that, in the relevant region in which the vortex patch was advected (central region of the blue box), the hydrostatic gradient (green vectors in Fig. 12b) was mostly weak or even opposing the total $\Delta p'$-gradient (Fig. 11b).

The pressure difference field in Fig. 11b also shows a dipole in the area of the vortex patch itself (x = -1.2 km and y = -0.7 km), indicating that the vortex patch in the EO simulations remained

Accepted for publication in *Monthly Weather Review*. DOI 10.1175/MWR-D-22-0026.1.

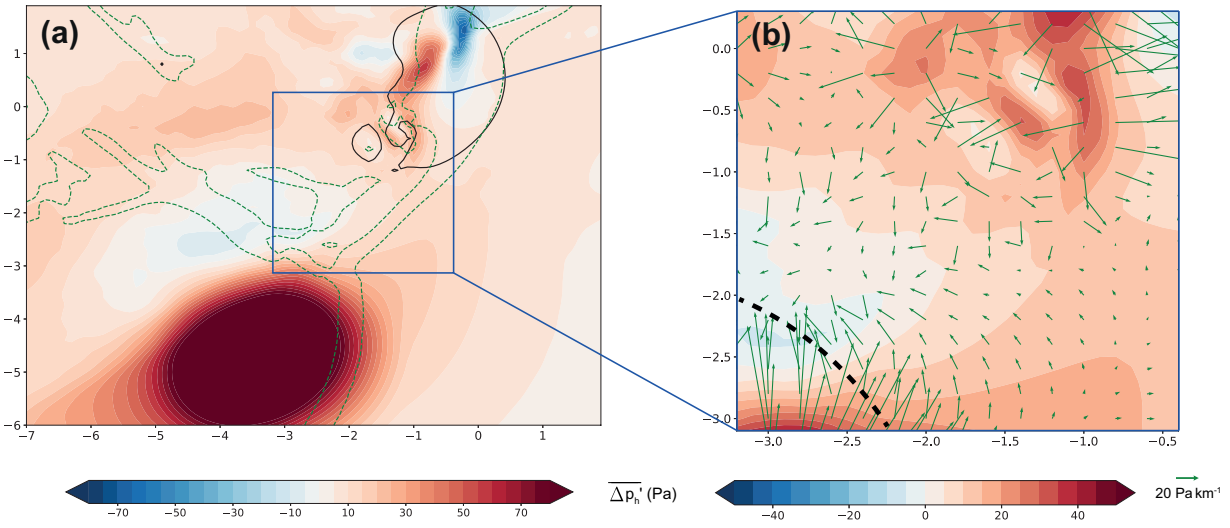

FIG. 12. As Fig. 11a,b but for the difference in the surface hydrostatic pressure ($p'_h = \int_{30m}^{\text{top}} \rho g \, dz + p_{\text{top}}$, with p_{top} being the pressure at the top of the domain) between the external outflow (EO) run and the control run, averaged between 3900 and 4500 s (shaded). The black dashed line indicates the approximate location of the gust front at 4500 s. The total p' difference in Fig. 11a is a result of this hydrostatic component and nonhydrostatic effects (e.g., Markowski and Richardson 2010).

farther northeast than in the control run, as already qualitatively observed in Figure 9. Except for in this dipole region, the average pressure gradient force was directed to the northeast in this area (green vectors in Fig. 11b). Likely attributable to this pressure gradient, the flow in which the vortex patch was embedded, had a smaller component away from the updraft (black vectors in Fig. 11b). This is supported by a simple evaluation of the pressure gradient acceleration term $\text{dv dt}^{-1} = -\rho^{-1}\nabla p$. Assuming $\rho = 1$ kg m^{-3}, an average p gradient of -5 to -10 Pa km^{-1} (Fig. 11a) over 10 min would result in a deceleration of a parcel by 3 to 6 m s^{-1}.

The idealized simulations in section 3a have shown that such a decrease in the motion speed of the vortex patch on the order of several meters per second can lead to tornadogenesis success. Therefore, it seems that the influence of the pressure field ahead of the external outflow boundary led to changes in the flow, ultimately leading to the the formation of a TLV.

A relevant analogy to the observed flow changes might be a stagnation point flow (e.g., Batchelor 2000, chapter 5.5), in which the horizontal flow encounters a rigid wall and is deflected perpendicular to the initial flow-direction, which requires a high-pressure perturbation. Here, the non-rigid external outflow boundary acted similarly to such a wall, albeit three-dimensionally and on a larger

Accepted for publication in *Monthly Weather Review*. DOI 10.1175/MWR-D-22-0026.1.

scale, generating pressure perturbations that decelerated and deflected the opposing flow several kilometers ahead. The results do not mean, however, that a well-defined boundary is always necessary for the proposed mechanism, since a pressure gradient can already result from hydrostatic pressure increase in the external outflow alone (Fig. 12). The contribution of hydrostatic effects on tornadogenesis was relatively small in the simulations but it might be more important in cases where no well-defined outflow boundary is impacting the supercell (e.g., Fig. 3a,b,c,e,f,g,h,i).

4. Discussion

a. Robustness of the idealized simulations

The idealized simulations in section 3a indicate that whether a near-ground vortex patch can intensify into a TLV can depend on the advection speed relative to the updraft, which is consistent with observations (e.g., Dowell and Bluestein 2002b; Tanamachi et al. 2012; Skinner et al. 2014) and previous simulations (e.g., Markowski and Richardson 2014; Guarriello et al. 2018; Murdzek et al. 2020; Gray and Frame 2021). Building on this argument, section 3b showed that the residence time of vortex patches in the updraft area could be increased by external outflow. Due to the locally fixed nature of the heat sinks and because the outflow from the pseudostorm blocked farther northward advancement of the external boundary, the external outflow never reached the TLV throughout the 2-h simulation time. Therefore, the simulation here can be seen as an ideal scenario, because negative effects of external outflow were mostly excluded. In many real cases, outflow of e.g., merging storms does ultimately seem to have a detrimental effect on the tornado, leading to subsequent tornado dissipation and storm weakening (e.g., Markowski et al. 1998; Wurman et al. 2007; Flournoy et al. 2022). The influence of external pressure perturbations on the flow found in this study could also play a role in this destructive scenario, for instance if developing vortices were forced out of the updraft area.

The robustness of the results was tested with additional simulations in the parameter space of Fischer and Dahl (2020). Variations of the EO run with other combinations of heat source and sink strengths, slightly different positions of the additional heat sink, or a breaking dam style heat sink that produced a straighter oriented density current, were performed. These cases were mostly consistent with the findings here. The only simulation that evolved differently was one with a very weak heat sink array ($S_{c0} = -0.006$ K s^{-1}). The initially much weaker vortex patches (than in the

Accepted for publication in *Monthly Weather Review*. DOI 10.1175/MWR-D-22-0026.1.

case presented here) did not form a TLV until the external outflow boundary reached the updraft area. At that point, it seems that vertical vorticity in the much stronger external outflow could be increased to TLV strength by the strong updraft. This could mean that in some cases vertical vorticity generation on the cool side of the external boundary could also be important.

b. Comparison of the different external factors for tornadogenesis

In this study, the percentage of supercells that were influenced by external storms or boundaries prior to tornadogenesis is even higher (around 80%) compared to previous studies (around 50% in Lee et al. 2006; Rogers and Weiss 2008, and 70% in Markowski 1998). Reasons for this increase could be that only initial supercell tornadoes were included here, and that not only one type of interaction was considered. It is important to realize that the significance of this and the above cited studies is weakened by the fact that the frequency of interactions in nontornadic storms is unknown, and could be similarly high over the same period (here 20 min). Since the focus of the present study was on the modeling side and the observations served mainly as a motivation, this problem is left for future studies. Nevertheless, the large percentage found herein is at least consistent with the different hypothesized mechanisms (as reviewed in section 1). In the present study, an additional mechanism is proposed, which relies on changes of the vortex-scale flow fields.

The relative importance of these different mechanisms is difficult to quantify. In many observed cases herein, tornadogenesis happened during a period when the high reflectivity region of an external storm continuously influenced the supercell, without overtaking it (e.g., Fig. 1). In others, the precipitation regions were fully merged before the circulation intensified and the tornado was reported (e.g., Figs. 1e,f). Such a variety in timing or relative location was also found in Markowski et al. (1998) and Lee et al. (2006), which might might suggest different mechanisms. For instance, the pressure field influence proposed in this study is more likely to be relevant in cases where tornadogenesis happened relatively early during the interaction (e.g., Fig. 3a,c,d).

Three final aspects are noteworthy. (i) A common perception is that isolated supercells tend to have the highest tornado potential, which at first seems to be contradicting the findings here. However, most interactions in this dataset impacted the supercells from the southwestern quadrant (Fig. 4a and Fig. 3c,d,h), which means that the supercell inflow was usually undisturbed. In other cases, the merging cells were often small or weak (e.g., Fig. 3b,e,f). Hence, it seems that a

Accepted for publication in *Monthly Weather Review*. DOI 10.1175/MWR-D-22-0026.1.

supercell needs to be "isolated enough" but some interactions of the right type could actually be beneficial. (ii) Local descending reflectivity cores (DRCs) or downbursts in the rear-flank outflow could have a similar effect as the external boundary in section 3b and change the flow structure favorably for tornadogenesis (e.g., Rasmussen et al. 2006; Byko et al. 2009). In fact, Markowski et al. (2012) observed a similar pressure gradient southwest of the developing tornado as shown here, but associated with a DRC. As suggested by Markowski et al. (2018), such an impact of storm-internal dynamics and microphysics would contribute to the complexity and weak internal predictability of tornadogenesis (see also Coffer et al. 2017; Flournoy et al. 2020; Markowski 2020). This, as well as external influences such as the ones discussed in this study (see also Dowell and Bluestein 2002b; Klees et al. 2016), are likely reasons for the variety of tornado outcomes that are possible in a given environment. (iii) Much of our current knowledge about tornadoes relies on computer simulations of supercells in horizontally homogeneous environments. Storm interactions are actively avoided in most of these studies by using a single, localized initiation (e.g., a warm bubble). It seems that many (first) tornadoes could depend on such interactions. Therefore, more research on non-isolated storms is warranted.

5. Summary

To complement the extant literature on supercell interactions with external boundaries and mergers, 136 supercell tornado cases were analyzed using WSR-88D radar data. A broad spectrum of interactions (storm merger events, as well as pre-existing storm-scale boundaries and outflow from neighboring storms) were included. In this dataset, 80% of supercell tornadoes happened during or after a period of such a storm-storm or storm-boundary interaction. Almost all interactions were estimated to occur within the southwestern quadrant of the supercell. Several common patterns of interactions were also identified, such as a chain of supercells, flanking-line convection, a QLCS or outflow boundary catching up to a supercell, and small inflow mergers. Although it remains unclear how many of these interactions were merely coincidental, these results support the idea that external factors can sometimes serve as catalysts for tornadogenesis.

In order to shed more light on the possible dynamics of these interactions, two sets of idealized simulations were performed in CM1, focusing on the vortex dynamics during tornadogenesis. The first experiment modeled the evolution of a pre-tornadic vortex patch into a tornado. It was

Accepted for publication in *Monthly Weather Review*. DOI 10.1175/MWR-D-22-0026.1.

shown that the near-ground updraft-relative flow has a direct effect on tornado potential. If the near-ground updraft-relative flow is relatively fast, the developing vortex remains in the region with largest vertical velocity gradient for a shorter time, limiting the stretching of vertical vorticity. Hence, the vortex tends to be weaker and more vertically tilted, both reducing tornado potential. Furthermore, these simulations may offer some insights into the characteristics of funnel clouds, showing that the associated vortex column can be strongly tilted and sometimes vary in intensity with height.

A second set of idealized simulations was performed to relate these results to the importance of supercell interactions. An external outflow was added to the southwest of a previously nontornadic pseudo-supercell. It was found that this resulted in a high pressure perturbation within the external outflow and several km downstream of the boundary, the latter being dominated by the dynamic pressure contribution. Since the outflow impacted the pseudo-supercell from the southwest, this led to a pressure gradient acceleration opposing the horizontal near-surface flow in the updraft region. Hence, the vertical vorticity rich supercell outflow air was able to remain beneath the main updraft in a region of horizontal convergence, which facilitated tornadogenesis in an otherwise nontornadic setup.

This mechanism can be seen as a possible catalyst for tornadogenesis, in addition to the ones previously suggested (e.g., enhanced convergence along outflow boundaries, updraft intensification via coalescence of two buoyant thermals, or more favorable mesoscale environments close to airmass boundaries). Which one of these factors is most relevant, or how common externally-instigated tornadogenesis really is, remain open questions.

Accepted for publication in *Monthly Weather Review*. DOI 10.1175/MWR-D-22-0026.1.

Acknowledgments. This research was supported by NSF Grant AGS-1651786. Dr. George Bryan is acknowledged for providing CM1. Alex Schueth and Billy Faletti were of essential help for the analysis and categorization of tornado cases. Thanks are also extended to Matt Flournoy as well as the two anonymous reviewers. Discussions with Dr. Chris Weiss, Dr. Matt Parker, Dr. Eric Bruning, and Cameron Nixon contributed to early stages of the study.

Data availability statement. The animations referred to in the text, the CM1 source code, namelist files, and a list of the tornado cases can be found online under the url github.com/Janfisch/FischerDahl2022 or upon request to the first author.

References

Atkins, N., M. L. Weisman, and L. J. Wicker, 1999: The influence of preexisting boundaries on supercell evolution. *Mon. Wea. Rev.*

Barnes, S. L., 1964: A Technique for Maximizing Details in Numerical Weather Map Analysis. *Journal of Applied Meteorology and Climatology*, **3 (4)**, 396–409, https://doi.org/10.1175/1520-0450(1964)003<0396:ATFMDI>2.0.CO;2, URL https://journals.ametsoc.org/view/journals/apme/3/4/1520-0450_1964_003_0396_atfmdi_2_0_co_2.xml.

Batchelor, G. K., 2000: *An Introduction to Fluid Dynamics*. Cambridge Mathematical Library, Cambridge University Press, https://doi.org/10.1017/CBO9780511800955.

Blanchard, D. O., 2008: Interactions between a supercell and a quasi-stationary frontal boundary. *Mon. Wea. Rev.*, **136 (12)**, 5199–5210, https://doi.org/10.1175/2008MWR2437.1.

Bluestein, H. B., K. J. Thiem, J. C. Snyder, and J. B. Houser, 2019: Tornadogenesis and early Tornado evolution in the El Reno, Oklahoma, supercell on 31 May 2013. *Mon. Wea. Rev.*, **147 (6)**, 2045–2066, https://doi.org/10.1175/MWR-D-18-0338.1.

Bluestein, H. B., and M. L. Weisman, 2000: The interaction of numerically simulated supercells initiated along lines. *Mon. Wea. Rev.*, **128 (9)**, 3128–3149, https://doi.org/10.1175/1520-0493(2000)128<3128:TIONSS>2.0.CO;2.

Bryan, G. H., and J. M. Fritsch, 2002: A benchmark simulation for moist nonhydrostatic numerical models. *Mon. Wea. Rev.*, **130 (12)**, 2917–2928, https://doi.org/10.1175/1520-0493(2002)1302.0.CO;2.

Byko, Z., P. Markowski, Y. Richardson, J. Wurman, and E. Adlerman, 2009: Descending Reflectivity Cores in Supercell Thunderstorms Observed by Mobile Radars and in a High-Resolution Numerical Simulation. *Wea. Forecasting*, **24 (1)**, 155–186, https://doi.org/10.1175/2008waf2222116.1.

Coffer, B. E., and M. D. Parker, 2015: Impacts of increasing low-level shear on supercells during the early evening transition. *Mon. Wea. Rev.*, **143 (5)**, 1945–1969, https://doi.org/10.1175/MWR-D-14-00328.1.

Coffer, B. E., and M. D. Parker, 2017: Simulated Supercells in Nontornadic and Tornadic VORTEX2 Environments. *Mon. Wea. Rev.*, **145 (1)**, 149–180, https://doi.org/10.1175/mwr-d-16-0226.1.

Coffer, B. E., and M. D. Parker, 2018: Is There a "Tipping Point" between Simulated Nontornadic and Tornadic Supercells in VORTEX2 Environments? *Mon. Wea. Rev.*, **146 (8)**, 2667–2693, https://doi.org/10.1175/mwr-d-18-0050.1.

Coffer, B. E., M. D. Parker, J. M. Dahl, L. J. Wicker, and A. J. Clark, 2017: Volatility of tornadogenesis: An ensemble of simulated nontornadic and tornadic supercells in VORTEX2 environments. *Mon. Wea. Rev.*, **145 (11)**, 4605–4625, https://doi.org/10.1175/MWR-D-17-0152.1.

Dahl, J. M. L., 2015: Near-Ground Rotation in Simulated Supercells: On the Robustness of the Baroclinic Mechanism. *Mon. Wea. Rev.*, **143 (12)**, 4929–4942, https://doi.org/10.1175/mwr-d-15-0115.1.

Dahl, J. M. L., 2020: Near-Surface Vortex Formation in Supercells from the Perspective of Vortex Patch Dynamics. *Mon. Wea. Rev.*, **148 (8)**, 3533–3547, https://doi.org/10.1175/MWR-D-20-0080.1.

Accepted for publication in *Monthly Weather Review*. DOI 10.1175/MWR-D-22-0026.1.

Dahl, J. M. L., M. D. Parker, and L. J. Wicker, 2014: Imported and storm-generated near-ground vertical vorticity in a simulated supercell. *J. Atmos. Sci.*, **71 (8)**, 3027–3051, https://doi.org/10.1175/JAS-D-13-0123.1.

Davies-Jones, R., 2015: A review of supercell and tornado dynamics. *Atmos. Res.*, **158-159**, 274–291, https://doi.org/10.1016/j.atmosres.2014.04.007.

Davies-Jones, R., and H. Brooks, 1993: Mesocyclogenesis from a Theoretical Perspective. *The Tornado: Its Structure, Dynamics, Prediction, and Hazards*, **79**, 105–114.

Davies-Jones, R. P., 1986: Tornado dynamics. *Thunderstorm morphology and dynamics*, **2**, 197–236.

Doswell, C. A., D. V. Baker, and C. A. Liles, 2002: Recognition of negative mesoscale factors for severe-weather potential: A case study. *Wea. Forecasting*, **17 (5)**, 937–954, https://doi.org/10.1175/1520-0434(2002)017<0937:RONMFF>2.0.CO;2.

Dowell, D. C., and H. B. Bluestein, 2002a: The 8 June 1995 McLean, Texas, storm. Part I: Observations of cyclic tornadogenesis. *Mon. Wea. Rev.*, **130 (11)**, 2626–2648, https://doi.org/10.1175/1520-0493(2002)130<2626:TJMTSP>2.0.CO;2.

Dowell, D. C., and H. B. Bluestein, 2002b: The 8 June 1995 McLean, Texas, storm. Part II: Cyclic tornado formation, maintenance, and dissipation. *Monthly Weather Review*, **130 (11)**, 2649–2670, https://doi.org/10.1175/1520-0493(2002)130<2649:TJMTSP>2.0.CO;2.

Droegemeier, K. K., and R. B. Wilhelmson, 1987: Numerical Simulation of Thunderstorm Outflow Dynamics. Part I: Outflow Sensitivity Experiments and Turbulence Dynamics. *J. Atmos. Sci.*

Fischer, J., and J. M. Dahl, 2022: Transition of Near-Ground Vorticity Dynamics During Tornadogenesis. *J. Atmos. Sci.*, **79**, 467–483, https://doi.org/10.1175/jas-d-21-0181.1.

Fischer, J., and J. M. L. Dahl, 2020: The Relative Importance of Updraft and Cold Pool Characteristics in Supercell Tornadogenesis Using Highly Idealized Simulations. *J. Atmos. Sci.*, **77 (12)**, 4089–4107, https://doi.org/10.1175/jas-d-20-0126.1.

Flournoy, M. D., M. C. Coniglio, E. N. Rasmussen, J. C. Furtado, and B. E. Coffer, 2020: Modes of storm-scale variability and tornado potential in VORTEX2 near- And far-

field tornadic environments. *Monthly Weather Review*, **148 (10)**, 4185–4207, https://doi.org/10.1175/MWR-D-20-0147.1.

Flournoy, M. D., A. W. Lyza, M. A. Satrio, M. R. Diedrichsen, M. C. Coniglio, and S. Waugh, 2022: A Climatology of Cell Mergers with Supercells and Their Association with Mesocyclone Evolution. *Monthly Weather Review*, **150 (2)**, 451–461, https://doi.org/10.1175/mwr-d-21-0204.1.

French, A. J., and M. D. Parker, 2012: Observations of mergers between squall lines and isolated supercell thunderstorms. *Weather and Forecasting*, **27 (2)**, 255–278, https://doi.org/10.1175/WAF-D-11-00058.1.

French, M. M., H. B. Bluestein, I. Popstefanija, C. A. Baldi, and R. T. Bluth, 2013: Reexamining the vertical development of tornadic vortex signatures in supercells. *Mon. Wea. Rev.*, **141 (12)**, 4576–4601, https://doi.org/10.1175/MWR-D-12-00315.1.

French, M. M., and D. M. Kingfield, 2019: Dissipation characteristics of tornadic vortex signatures associated with long-duration tornadoes. *Journal of Applied Meteorology and Climatology*, **58 (2)**, 317–339, https://doi.org/10.1175/JAMC-D-18-0187.1.

Golden, J. H., and D. Purcell, 1977: Photogrammetric Velocities for the Great Bend, Kansas, Tornado of 30 August 1974: Accelerations and Asymmetries. *Mon. Wea. Rev.*, **105 (4)**, 485–492, https://doi.org/10.1175/1520-0493(1977)105<0485:PVFTGB>2.0.CO;2.

Goodman, S. J., and K. R. Knupp, 1993: Tornadogenesis via squall line and supercell interaction: The November 15, 1989, Huntsville, Alabama, Tornado. *Washington DC American Geophysical Union Geophysical Monograph Series*, **79**, 183–199, https://doi.org/10.1029/GM079p0183.

Gray, K., and J. Frame, 2021: The Impact of Midlevel Shear Orientation on the Longevity of and Downdraft Location and Tornado-like Vortex Formation within Simulated Supercells. *Mon. Wea. Rev.*

Griffin, C. B., D. J. Bodine, J. M. Kurdzo, A. Mahre, and R. D. Palmer, 2019: High-temporal resolution observations of the 27 May 2015 Canadian, Texas, Tornado using the atmospheric imaging radar. *Mon. Wea. Rev.*, **147 (3)**, 873–891, https://doi.org/10.1175/MWR-D-18-0297.1.

Guarriello, F., C. J. Nowotarski, and C. C. Epifanio, 2018: Effects of the Low-Level Wind Profile on Outflow Position and Near-Surface Vertical Vorticity in Simulated Supercell Thunderstorms. *J. Atmos. Sci.*, **75 (3)**, 731–753, https://doi.org/10.1175/jas-d-17-0174.1.

Hamilton, R. E., 1969: *A review of use of radar in detection of tornadoes and hail*. US Department of Commerce, Environmental Science Service Administration.

Hastings, R., and Y. Richardson, 2016: Long-term morphological changes in simulated supercells following mergers with nascent supercells in directionally varying shear. *Mon. Wea. Rev.*, **144 (2)**, 471–499, https://doi.org/10.1175/MWR-D-15-0193.1.

Helmus, J., and S. Collis, 2016: The Python ARM Radar Toolkit (Py-ART), a Library for Working with Weather Radar Data in the Python Programming Language. *Journal of Open Research Software*, **4**, https://doi.org/10.5334/jors.119.

Honda, T., and T. Kawano, 2016: A possible mechanism of tornadogenesis associated with the interaction between a supercell and an outflow boundary without horizontal shear. *J. Atmos. Sci.*, **73 (3)**, 1273–1292, https://doi.org/10.1175/JAS-D-14-0347.1.

Klees, A. M., Y. P. Richardson, P. M. Markowski, C. Weiss, J. M. Wurman, and K. K. Kosiba, 2016: Comparison of the Tornadic and Nontornadic Supercells Intercepted by VORTEX2 on 10 June 2010. *Mon. Wea. Rev.*, **144 (9)**, 3201–3231, https://doi.org/10.1175/mwr-d-15-0345.1.

Lee, B. D., B. F. Jewett, and R. B. Wilhelmson, 2006: The 19 April 1996 Illinois Tornado Outbreak. Part II: Cell Mergers and Associated Tornado Incidence. *Wea. Forecasting*, **21 (4)**, 449–464.

Lemon, L. R., 1976: The Flanking Line, a Severe Thunderstorm Intensification Source. *J. Atmos. Sci.*, **33**, 686–694.

Lemon, L. R., D. W. Burgess, and R. A. Brown, 1975: Tornado production and storm sustenance. *BULLETIN OF THE AMERICAN METEOROLOGICAL SOCIETY*, AMER METEOROLOGICAL SOC 45 BEACON ST, BOSTON, MA 02108-3693, Vol. 56, 744–745.

Lewellen, W. S., 1971: A review of confined vortex flows. *National Aeronautics and Space Administration*.

Accepted for publication in *Monthly Weather Review*. DOI 10.1175/MWR-D-22-0026.1.

Maddox, R. A., Hoxit, and Chappell, 1980: A Study of Tornadic Thunderstorm Interactions with Thermal Boundaries. *Mon. Wea. Rev.*

Magee, K. M., and C. E. Davenport, 2020: An observational analysis quantifying the distance of supercell-boundary interactions in the great plains. *Journal of Operational Meteorology*, **8 (2)**, 15–38, https://doi.org/10.15191/nwajom.2020.0802.

Markowski, P., and C. Hannon, 2006: Multiple-Doppler radar observations of the evolution of vorticity extrema in a convective boundary layer. *Mon. Wea. Rev.*, **134 (1)**, 355–374, https://doi.org/10.1175/MWR3060.1.

Markowski, P., and Y. Richardson, 2010: *Mesoscale meteorology in midlatitudes*, Vol. 2. John Wiley and Sons.

Markowski, P., Y. Richardson, and G. Bryan, 2014: The Origins of Vortex Sheets in a Simulated Supercell Thunderstorm. *Mon. Wea. Rev.*, **142 (11)**, 3944–3954, https://doi.org/10.1175/mwr-d-14-00162.1.

Markowski, P., and Coauthors, 2012: The pretornadic phase of the Goshen County, Wyoming, supercell of 5 June 2009 intercepted by VORTEX2. Part I: Evolution of kinematic and surface thermodynamic fields. *Mon. Wea. Rev.*, **140 (9)**, 2887–2915, https://doi.org/10.1175/MWR-D-11-00336.1.

Markowski, P. M., 2020: What is the intrinsic predictability of tornadic supercell thunderstorms? *Mon. Wea. Rev.*, **148 (8)**, 3157–3180, https://doi.org/10.1175/mwr-d-20-0076.1.

Markowski, P. M., T. P. Hatlee, and Y. P. Richardson, 2018: Tornadogenesis in the 12 May 2010 Supercell Thunderstorm Intercepted by VORTEX2 near Clinton, Oklahoma. *Mon. Wea. Rev.*, **146 (11)**, 3623–3650, https://doi.org/10.1175/mwr-d-18-0196.1.

Markowski, P. M., E. N. Rasmussen, and J. M. Straka, 1998: The occurrence of Tornadoes in supercells interacting with boundaries during VORTEX-95. *Wea. Forecasting*, **13 (3 PART2)**, 852–859, https://doi.org/10.1175/1520-0434(1998)013<0852:tootis>2.0.co;2.

Markowski, P. M., and Y. P. Richardson, 2014: The Influence of Environmental Low-Level Shear and Cold Pools on Tornadogenesis: Insights from Idealized Simulations. *J. Atmos. Sci.*, **71 (1)**, 243–275, https://doi.org/10.1175/jas-d-13-0159.1.

Markowski, P. M., and Y. P. Richardson, 2017: Large Sensitivity of Near-Surface Vertical Vorticity Development to Heat Sink Location in Idealized Simulations of Supercell-Like Storms. *J. Atmos. Sci.*, **74 (4)**, 1095–1104, https://doi.org/10.1175/jas-d-16-0372.1.

Murdzek, S. S., P. M. Markowski, Y. P. Richardson, and R. L. Tanamachi, 2020: Processes preventing the development of a significant tornado in a Colorado supercell on 26 May 2010. *Mon. Wea. Rev.*, **148 (5)**, 1753–1778, https://doi.org/10.1175/MWR-D-19-0288.1.

Nowotarski, C. J., P. M. Markowski, Y. P. Richardson, and G. H. Bryan, 2014: Supercell Low-Level Mesocyclones in Simulations with a Sheared Convective Boundary Layer. *Mon. Wea. Rev.*, **143 (1)**, 272–297, https://doi.org/10.1175/mwr-d-14-00151.1.

Parker, M. D., and J. M. L. Dahl, 2015: Production of Near-Surface Vertical Vorticity by Idealized Downdrafts. *Mon. Wea. Rev.*, **143 (7)**, 2795–2816, https://doi.org/10.1175/mwr-d-14-00310.1.

Purdom, J. F. W., 1976: Some uses of high-resolution GOES imagery in the mesoscale forecasting of convection and its behavior. *Mon. Wea. Rev.*, **104 (12)**, 1474–1483.

Rasmussen, E. N., S. Richardson, J. M. Straka, P. M. Markowski, and D. O. Blanchard, 2000: The association of significant tornadoes with a baroclinic boundary on 2 June 1995. *Mon. Wea. Rev.*, **128 (1)**, 174–191, https://doi.org/10.1175/1520-0493(2000)128<0174:TAOSTW>2.0.CO;2.

Rasmussen, E. N., J. M. Straka, M. S. Gilmore, and R. Davies-Jones, 2006: A Preliminary Survey of Rear-Flank Descending Reflectivity Cores in Supercell Storms. *Wea. Forecasting*, **21 (6)**, 923–938, https://doi.org/10.1175/waf962.1.

Rogers, J. W., and C. C. Weiss, 2008: The association of cell mergers with tornado occurrence. *24th Conf. on Severe Local Storms*, 3–23.

Skinner, P. S., C. C. Weiss, M. M. French, H. B. Bluestein, P. M. Markowski, and Y. P. Richardson, 2014: VORTEX2 Observations of a Low-Level Mesocyclone with Multiple Internal Rear-Flank Downdraft Momentum Surges in the 18 May 2010 Dumas, Texas, Supercell*. *Mon. Wea. Rev.*, **142 (8)**, 2935–2960, https://doi.org/10.1175/mwr-d-13-00240.1.

Tanamachi, R. L., H. B. Bluestein, J. B. Houser, S. J. Frasier, and K. M. Hardwick, 2012: Mobile, X-band, polarimetric doppler radar observations of the 4 May 2007 Greensburg, Kansas,

Tornadic Supercell. *Monthly Weather Review*, **140 (7)**, 2103–2125, https://doi.org/10.1175/MWR-D-11-00142.1.

Tanamachi, R. L., H. B. Bluestein, M. Xue, W. C. Lee, K. A. Orzel, S. J. Frasier, and R. M. Wakimoto, 2013: Near-surface vortex structure in a tornado and in a sub-tornado-strength convective-storm vortex observed by a mobile, w-band radar during VORTEX2. *Monthly Weather Review*, **141 (11)**, 3661–3690, https://doi.org/10.1175/MWR-D-12-00331.1.

Tanamachi, R. L., P. L. Heinselman, and L. J. Wicker, 2015: Impacts of a storm merger on the 24 May 2011 El Reno, Oklahoma, tornadic supercell. *Wea. Forecasting*, **30 (3)**, 501–524, https://doi.org/10.1175/WAF-D-14-00164.1.

Tao, W.-K., and J. Simpson, 1984: Cloud Interactions and Merging: Numerical Simulations. *J. Atmos. Sci.*, **41 (19)**, 2901–2917, https://doi.org/10.1175/1520-0469(1984)041<2901:CIAMNS>2.0.CO;2.

Thompson, R. L., and R. Edwards, 2000: An overview of environmental conditions and forecast implications of the 3 May 1999 Tornado outbreak. *Wea. Forecasting*, **15 (6)**, 682–699, https://doi.org/10.1175/1520-0434(2000)015<0682:AOOECA>2.0.CO;2.

Weiss, C. C., D. C. Dowell, J. L. Schroeder, P. S. Skinner, A. E. Reinhart, P. M. Markowski, and Y. P. Richardson, 2015: A comparison of near-surface buoyancy and baroclinity across three VORTEX2 supercell intercepts. *Mon. Wea. Rev.*, **143 (7)**, 2736–2753, https://doi.org/10.1175/MWR-D-14-00307.1.

Westcott, N., 1984: A Historical Perspective on Cloud Mergers. *Bulletin of the American Meteorological Society*, **65 (3)**, 219–227, https://doi.org/10.1175/1520-0477(1984)065\textless{}0219:AHPOCM\textgreater{}2.0.CO;2.

Wilkins, E. M., Y. K. Sasaki, G. E. Gerber, and W. H. Chaplin, 1976: Numerical Simulation of the Lateral Interactions Between Buoyant Clouds. *J. Atmos. Sci.*, **33 (7)**, 1321–1329, https://doi.org/10.1175/1520-0469(1976)033<1321:NSOTLI>2.0.CO;2.

Wurman, J., Y. Richardson, C. Alexander, S. Weygandt, and P. F. Zhang, 2007: Dual-Doppler and single-Doppler analysis of a tornadic storm undergoing mergers and repeated tornadogenesis. *Mon. Wea. Rev.*, **135 (3)**, 736–758, https://doi.org/10.1175/MWR3276.1.